

This is the accepted manuscript made available via CHORUS. The article has been published as:

Rainbow Trapping with Long Oscillation Lifetimes in Gradient Magnetoinductive Metasurfaces

Zhixia Xu, Jun Shi, Robert J. Davis, Xiaoxing Yin, and Daniel F. Sievenpiper

Phys. Rev. Applied **12**, 024043 — Published 21 August 2019

DOI: [10.1103/PhysRevApplied.12.024043](https://doi.org/10.1103/PhysRevApplied.12.024043)

Rainbow trapping with long oscillation life-time in gradient magnetoinductive metasurfaces

Zhixia Xu^{1,2,*}, Jun Shi^{3,†}, Robert J. Davis², Xiaoxing Yin^{1,‡}, and Daniel F. Sievenpiper^{2,§}

¹ State Key Laboratory of Millimeter Waves, Southeast University, Nanjing 210096, China

² Electrical and Computer Engineering Department, University of California, San Diego,
California 92093, USA

³ Department of Electrical Engineering, California Institute of Technology, Pasadena,
California 91125 USA

*Zhixia Xu: 230159363@seu.edu.cn;

†Jun Shi: shijun@caltech.edu;

‡Xiaoxing Yin: 101010074@seu.edu.cn;

§Daniel F. Sievenpiper: dsievenpiper@eng.ucsd.edu.

Abstract

We report a gradient metasurface design at microwave bands as an elegant approach to realize the goal of ‘rainbow trapping’ for storage of waves, involving wave localization and absorption phenomena. A longitudinally placed coplanar waveguide are loaded with gradient metasurfaces on both sides, where split-ring resonators (SRRs) are the basic cell. Same SRRs are arranged along the transverse direction to establish magnetoinductive (MI) channels. Waves of different frequencies are coupled to corresponding SRRs at different positions in metasurfaces. Resonant trapping with a long oscillation life-time enhances the absorption caused by inherent losses of the materials, thereby suppressing reflections. Both simulations and measurements verify the existence of ‘rainbow trapping’. The proposed strategy enhances the interaction between waves and matters, opening an avenue for further component designs, including absorptive filters, multiplexers, and buffers.

Introduction

Rainbow trapping can be regarded as a phenomenon where propagating waves of different wavelengths are spatially separated, mimicking the separation of colors when light transmits through a prism. Since the first theoretical proposal of the rainbow trapping in metamaterials(1), many metamaterials have been designed to observe similar interesting phenomena(2–8). Beyond understanding fundamental properties, researches have been exploring this topic in large part because of the potential applications: the enhanced wave-matter interaction characteristic can be used to design broadband optical absorbers based on gradual structures(9, 10) as well as nonlinear optical devices(11–14); the spectrum splitting characteristic gives an alternative approach to designing wavelength division multiplexers utilized in antenna feeding networks(15, 16); the localization characteristic can potentially bring revolutionary changes to wave focusing (16, 17).

Most of previous works can be classified as dispersion engineering, where waveguides with tailored dispersion characteristics are the key to make waves of different wavelengths halt at desirable positions. Gratings were widely utilized to slow down surface plasmons to a standstill to obtain the rainbow trapping (18–21). Similar phenomena were also reported in photonic crystals(22–24) as well as metal-insulator-metal taper plasmonic waveguides(16). However, taking material loss and energy leakage into consideration, pioneers found a troubling phenomenon where rainbow trapping could suffer from strong coupling between forward and backward modes, such that it may be impossible to completely stop the light unless using special materials(25–28). In order to achieve true rainbow trapping with fully stopped light, tapered magnetic fields have been utilized in nonreciprocal waveguides(29). However, these designs rely on the use of gyromagnetic material and an external magnetic field to achieve the desired property, which increases the complexity of the system. It is therefore clear that further researches are needed to overcome the reflected waves in rainbow trapping within a broadband spectrum. Since loss and dispersion are two inherent features of materials, it is natural to consider utilizing ohmic loss to absorb unwanted signals to break couplings between forward and backward waves. Frequency selective surfaces were designed to utilize inherent loss of unit cells to absorb energy(30). And reflectionless filters are becoming mature in recent circuits researches, where resonators are usually loaded with resistors(31–34) to absorb backward waves. Without complex loaded networks, recent works also utilize loss in dielectrics and metals to suppress backward reflections(35, 36). In these designs, absorption performance relies on the position of resonators, where distance between neighboring artificial transmission lines need to be sufficiently large to obtain desirable performance, increasing the size of device.

In this work, a different strategy is proposed to achieve the broadband rainbow trapping, suppressing reflections and trapping waves of different frequencies at different positions. We apply the concept of gradient metasurfaces(37–40), which is widely used in scattering problems, to the transmission problem. We develop a hybrid transmission system: a coplanar waveguide (CPW) supporting a quasi-transverse electromagnetic (Q-TEM) mode whose ground planes on both sides are gradient-modified by magnetoinductive (MI) metasurfaces. Gradient MI metasurfaces are made up of gradient split-ring resonators (SRRs) whose geometric parameters adiabatically change along the longitudinal direction to obtain different frequency responses at different positions. Inherent loss in the metal and the dielectric substrate is the primary mechanism to suppress backward waves. It is foreseeable that by controlling the number of gradient SRRs operating at different frequencies along the longitudinal direction, we can arbitrarily control the working bandwidth, and by tailoring the number of SRRs along the transverse direction, we can even manipulate the zone where rainbow trapping happens. CST microwave studio was used to simulate S-parameters, field distributions, and loss analysis, and from detected time domain signals, we could investigate the oscillation life-time of trapped modes. To verify the simulations, a sample was fabricated, where we further used a network analyzer to measure the S-parameters and conduct near-field scanning. It should be

mentioned that because of the existence of non-radiating anapole mode, dielectric particles have potentials to be the alternative unit cell to trap energy at optical band(41–43). But it is quite challenging to excite the mode(44). Thus, once finding appropriate coupling method in waveguide systems, we can further design gradient metasurfaces based on dielectric particles to realize true rainbow trapping effect at optical band. The controllable zone, bandwidth, and reflectionless features all have potential usefulness in future devices based on the concept of rainbow trapping.

Results and Discussions

A. Structure designs

The proposed topology is shown in Fig. 1(a). We consider a normal waveguide placed along the longitudinal direction, with two gradient metasurfaces attached on both sides. In this work, every transverse MI channel consists of SRRs with identical geometric parameters, operating at the same frequency. Thus, signals of different frequencies are guided in different MI channels. These MI channels can be regarded as strong resonant channels where the effect of ohmic loss becomes prominent. Compared to a mechanical topology using only one mass-spring resonator along the transverse direction(7), this work uses resonator chains to establish MI channels to make the trapped ‘rainbow’ interact more strongly with the surrounding environment. In this case, ohmic losses will be enhanced to suppress the reflection. Besides enhanced ohmic losses in resonant MI channels, another key to suppressed reflection is the arrangement method. Despite the square lattice, transverse MI strength is bit stronger than longitudinal MI strength due to the gradual change of the response frequency of neighboring MI channels. That means the preferred route of coupling waves is transverse direction, orthogonal to the waveguide. Thus, the reflection signals can be further suppressed. As a comparison, without utilizing the transverse transmission, it becomes difficult to overcome reflected signals in previous SRR-loaded transmission line designs(45). Fig. 1(b) shows the detailed structure of the model operating at microwave bands in further simulations and measurements, where the array of SRRs are etched above the CPW. The near-field couplings happen near the slots. To people familiar with tensor impedance metasurfaces, the structure might be associated with sandwich-like impedance surface waveguides(46–49). The key difference is the resonance. Impedance waveguides do not rely on resonance. Different impedance surfaces on both sides of interface suppress transverse surface waves to establish waveguides and gradient changing of impedance further controls the propagation of surface waves. In this design, different parts of the gradient metasurface perform at different frequencies. Only within the resonant band, waves can be coupled into metasurfaces. When out of the resonant band, MI metasurfaces become transparent to the waves.

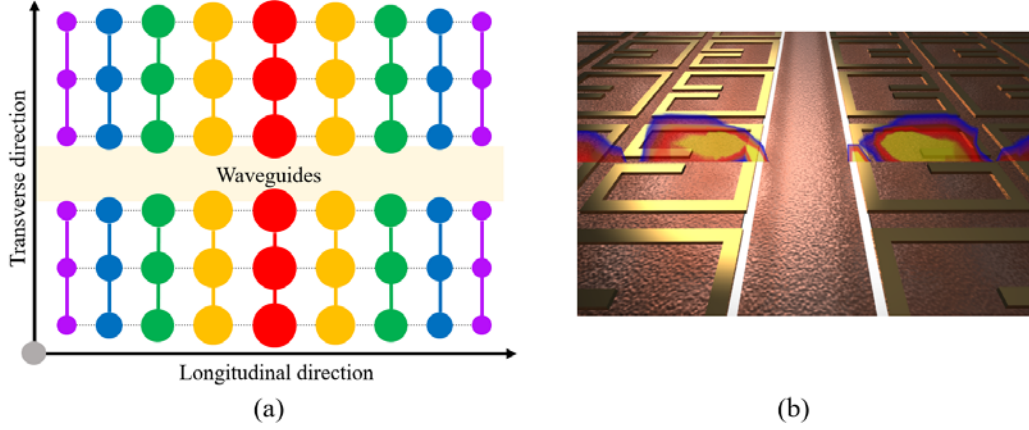


Fig. 1. (a) The proposed rainbow trapping topology, where solid lines represent strong couplings and dash lines represent weak couplings. (b) Detailed structure where the CPW is etched on one side of the substrate (brown) and loaded SRRs are etched on the other side (gold).

The whole structure is shown in Fig. 2. The CPW is etched on one side and metasurfaces are etched on the other side of a Rogers 4350B substrate of 0.762 mm thickness whose permittivity is 3.66 and loss tangent is 0.0037. The total length of the structure L is 120 mm, the width W is 33 mm, and the section of CPW without loaded metasurfaces L_I is 11.4 mm. The geometric parameters of the CPW are listed as: w_g is 15.3 mm, w_i is 2 mm, and w_s is 0.2 mm. The geometric parameters of metasurfaces are listed as: d is 2.5 mm, a is 2.2 mm, w_l is 0.2 mm, s is 0.2 mm, and L_f is changing on a gradient from 0.7 mm to 1.6 mm along x -axis (longitudinal direction), which is the key element to trap waves of different frequencies in different parts. The distance of the center of first row of SRRs to the center of CPW middle strip w_c is 1.9 mm. Q-factor of an individual SRR unit cell is around 250, obtained by the eigenmode solver of CST microwave studio. The value is common to patch resonators at microwave band(50, 51). Simulated electric field distributions 1 mm above the structure at typical frequencies are shown in Fig. 5 (a) to illustrate the rainbow trapping. Considering the symmetry, we only show results when energy is input into one port ($x = -60$ mm). Waves with different frequencies are trapped in different MI channels at different positions. Further, we conducted a loss analysis and found that losses in the substrate and copper are the two dominant sources of absorption, while the radiation loss is negligible.

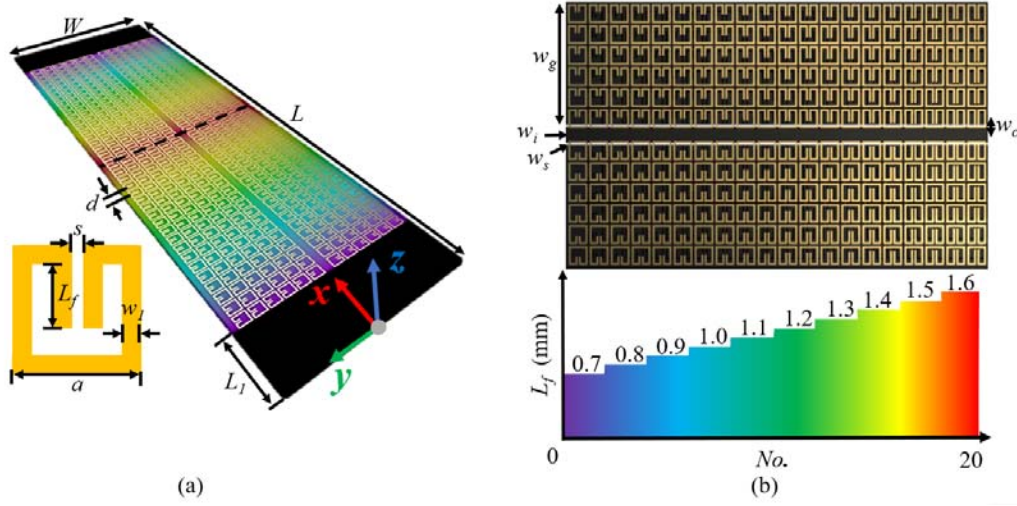


Fig. 2. The geometry of the proposed transmission line system consisting of CPW and MI metasurfaces.

B. Simulations and Measurements

The fabricated sample with SMA connectors is shown in Fig. 3(a), where the gradient metasurfaces are etched on the top layer and the CPW is etched on the bottom layer. The operating frequency ranges approximately from 8 GHz to 10 GHz. From the simulation results, we distinguished losses coming from different sources, including ohmic losses and radiation losses, as shown in Fig. 3(b). Ohmic loss in the dielectric and metal accounts for the largest portion, while radiation loss is negligible. About 60% of total input energy from one terminal is absorbed by dielectric substrate, and 40% is absorbed by metallic patch. Thus, most input power dissipates as heat in metasurfaces. Compared to low-loss transmission state of CPW, the absorption of the gradient metasurface is perfect. The remarkable absorption is brought by the resonant energy storage accompanied by long-time oscillation among unit cells, and the localized electromagnetic field in unit cells further enhance the absorption(52, 53).

Further, we used a network analyzer (N5242A) to measure S-parameters to check the transmission and reflection characteristics of the structure. S_{11} and S_{21} are shown in Fig. 3(c) and Fig. 3(d), respectively. Simulated and measured curves match well overall. Within the operating band, S_{11} stays below about -10 dB, while S_{21} is below about -20 dB, supporting the fact that most energy is dissipated in MI channels. There exist some discrepancies between simulated and measured results, which is caused by simulation and fabrication errors. The time-domain solver used here is really difficult to get perfect convergence due to the long-term time-domain signals of resonant states of the low-loss materials, thus, simulated curves, especially within the resonant band, will have some acceptable errors. Besides, the resonant performance is sensitive to geometric parameters, and the fabrication error is inevitable. A bit of reflection within the resonant band is inevitable because the coupling between metasurfaces and CPW influences the characteristic impedance. Due to the resonance, S-parameters' curves fluctuate impetuously. Here, we can tune the overlap of the MI metasurface and the

slot of CPW to tailor the coupling. It is a trade-off between the reflection and absorption. If coupling is too strong, the impedance of CPW change abruptly. MI metasurfaces don't work, only the nearest SRRs at both slots of CPW make sense, and the design acts as a traditional SRRs-load reflective filter(45). When we decrease the coupling, the impedance doesn't change too abruptly, most energy can permeate into MI metasurfaces and be absorbed. But, when we further decrease the coupling, almost no energy can be coupled to MI metasurfaces, the device doesn't work anymore.

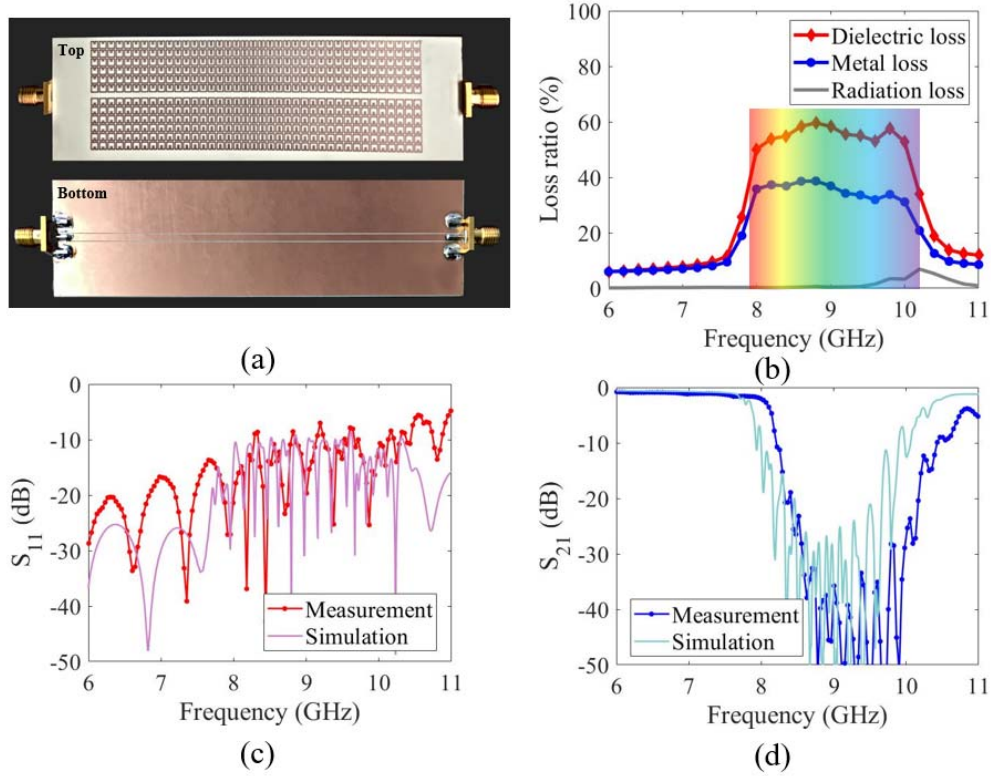


Fig. 3. (a) Photograph of fabricated sample. (b) Loss analysis. Measured and simulated (c) S_{11} and (d) S_{21} .

Note that the number of unit cells in the transverse direction (N_t) is set as 6 in this example. Usually, we can increase the absorption area to improve the performance of this device, especially the impedance matching. As shown in Fig. 4, S_{11} is more sensitive to N_t , compared to S_{21} . When N_t increases from 2 to 10, S_{11} decreases. There is probably a trade-off between the transverse size of MI metasurface and impedance matching at terminals. Here, we set N_t as 6 to keep S_{11} around -10 dB and the size is not too large.

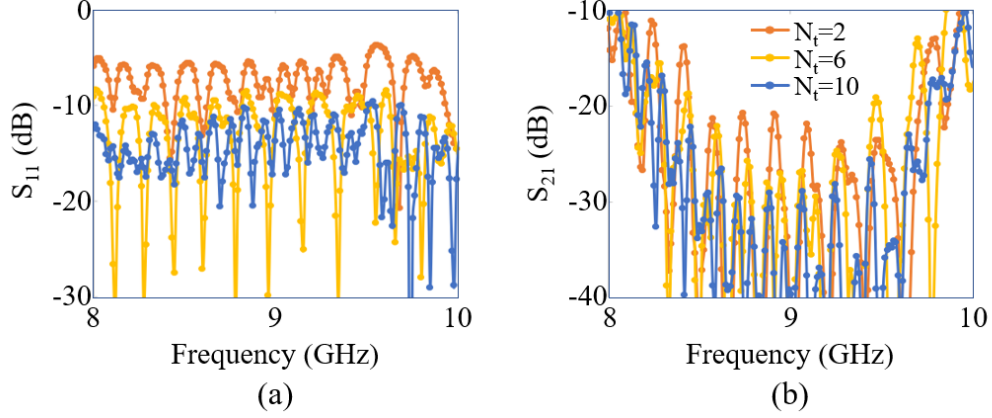


Fig. 4. S-parameters of designs with different N_t (a) S_{11} and (b) S_{21} .

In order to observe the distribution of the trapped ‘rainbow’, we analyzed the field distribution as well as time domain signals at different positions. The simulated electric field distributions at 8.2 GHz, 8.8 GHz, and 10 GHz are presented in Fig. 5(a), where waves of different frequencies are located at different positions. Field distributions in corresponding MI channels differ from each other. If we neglect longitudinal MI strength, the analysis can be simplified. The wavevector of MI is k , lattice constant of a square lattice being d . The current on n^{th} , $(n-1)^{\text{th}}$, and $(n+1)^{\text{th}}$ elements have the following relationships in MI channels, where ω is the angular frequency, Z_0 is the self-impedance of each element, and M is the mutual inductance(54, 55),

$$I_n = I_{n-1}e^{-jkd} \quad (1)$$

$$Z_0 I_n + j\omega M(I_{n-1} + I_{n+1}) = 0 \quad (2)$$

Two terminals of each MI channel could be assumed as open terminals. Hence, current distributions could be regarded as linear combinations of eigenstates with open boundary conditions. The currents can be assumed vary sinusoidally between two terminals. Hence, the l^{th} eigenvector in n^{th} element could be written as(56, 57),

$$I_n^{(l)} = I_0 \sin\left(\frac{nl\pi}{N+1}\right) \quad (3)$$

Thus, it is reasonable to observe that electromagnetic field is localized strongly in some elements while fields in other neighboring elements are weak.

We further investigated time-domain signals at the middle of different MI channels to evaluate the trapping ability in Fig. 5(b). The excitation was designed to be a Gaussian modulated wave. In order to record the evolution of electric signals, we set several ideal probes along the x-direction, parallel to the split, which is the orientation of the strongest components of electric vectors in an SRR. Although the excitation signal can be seen to end before 1 ns, extended ringing of signals can be overserved well even after 15 ns, proving the fact that the lasting trapping effects happen in these resonant MI channels. We can also see envelopes of signals decay with time due to the existence of damping. That means the ‘rainbow’ is really trapped in the MI channels

and interacts sufficiently with the surrounding environment, giving a possible solution to achieve the true rainbow trapping with suppressed reflection.

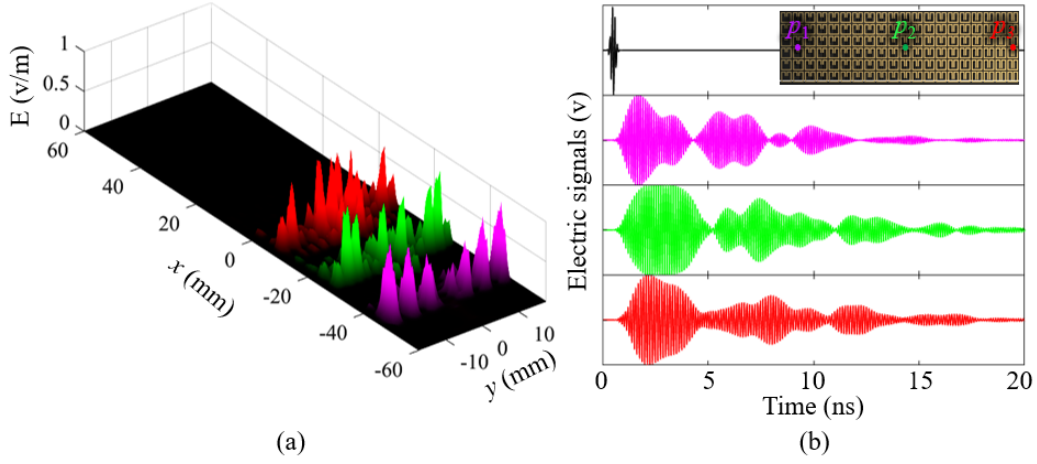


Fig. 5. (a) Simulated electric field distributions at different frequencies, 8.2 GHz (red), 8.8 GHz (green), and 10 GHz (pink). (b) Time domain signals, the excitation signal (black), signal at P_1 (pink), P_2 (green), and P_3 (red).

Fig. 6(a) shows the photograph of the near-field scanning, one port of the sample is connected to a broadband load and the other port of the sample is connected to one port of network analyzer whose second port is connected to the electric probe. The energy is input at the left terminal in figures of measured results. It is clearly to find that waves of different frequencies are trapped at different positions, which is the key property of this gradient MI metasurface. The fluctuation of field strength along the longitudinal direction indicates a mix of travelling waves and standing waves. But it is still difficult to estimate the matching property precisely. And we can only evaluate reflection from terminals, as shown in Fig. 3. Due to the limitations of the equipment, we could only measure the electric field along z -axis. Therefore, it may be a bit difficult to identify total electric field, for the reason that the main electric field of each SRR is along the x -axis around each split instead of along the z -axis. Due to the symmetry, if we excite the structure from another port, it is foreseeable to get the same result.

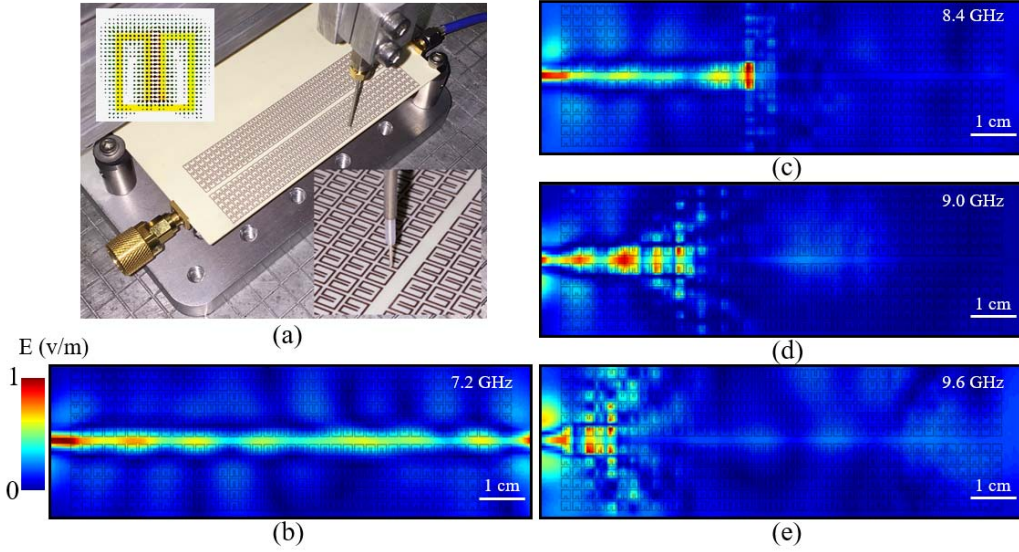


Fig. 6. (a) The near-field scanning experiments where two insets show the detail of the electric probe and electric field distribution of SRRs, respectively. Measured electric field distributions at (b) 7.2 GHz, (c) 8.4 GHz, (d) 9.0 GHz, (e) 9.6 GHz.

Conclusion

In conclusion, the proposed structure takes advantage of the gradient MI metasurface and a CPW to highlight potential advantages of the rainbow trapping with suppressed reflection at the input port. Different from previous designs realizing rainbow trapping based on gradual dispersion of metamaterials, the proposed structure utilizes gradual resonant channels to trap waves with a long oscillation life-time, enhancing the interactions between waves and the structure. And further, inherent losses of materials are utilized to absorb the trapped energy sufficiently. The proposed design can simplify the absorptive filter designs, which is commonly loaded with complex resistor networks. And we can further use this structure to design compact multiplexers. Moreover, by carefully changing loaded metasurfaces periodically, we may generate spatial harmonic waves to design leaky wave antennas. Although simulations and experiments were conducted at microwave bands, such a phenomenon could be exploited in device designs from mechanical waves all way to photonics, targeted towards applications in absorptive filters, antennas, optical buffers, and multiplexers.

Acknowledgments

Zhixia Xu and Jun Shi contributed equally to this work. The authors also acknowledge discussions with Shufan Wang and Yun Zhou. This work was supported by National Natural Science Foundation of China (Nos. 61771127 and 61427801), Scientific Research Foundation of Graduate School of Southeast University (No. YBJJ1814), and Postgraduate Research & Practice Innovation Program of Jiangsu Province (No. KYCX18_0098) as well as AFOSR contract FA9550-16-1-0093.

References

1. K. L. Tsakmakidis, A. D. Boardman, O. Hess, "Trapped rainbow" storage of light in metamaterials. *Nature*. **450**, 397–401 (2007).
2. P. Celli, B. Yousefzadeh, C. Daraio, S. Gonella, Bandgap widening by disorder in rainbow metamaterials. *Appl. Phys. Lett.* **114**, 091903 (2019).
3. P. Li, L. Cheng, Shear horizontal wave propagation in a periodic stubbed plate and its application in rainbow trapping. *Ultrasonics*. **84**, 244–253 (2018).
4. V. N. Smolyaninova, I. I. Smolyaninov, A. V. Kildishev, V. M. Shalaev, Experimental observation of the trapped rainbow. *Appl. Phys. Lett.* **96**, 211121 (2010).
5. M. Strebel, T.-O. Müller, B. Ruff, F. Stienkemeier, M. Mudrich, Quantum rainbow scattering at tunable velocities. *Phys. Rev. A*. **86**, 062711 (2012).
6. N. Jiménez, V. Romero-García, V. Pagneux, J.-P. Groby, Rainbow-trapping absorbers: Broadband, perfect and asymmetric sound absorption by subwavelength panels for transmission problems. *Sci. Rep.* **7**, 13595 (2017).
7. E. A. Skelton, R. V. Craster, A. Colombi, D. J. Colquitt, The multi-physics metawedge: graded arrays on fluid-loaded elastic plates and the mechanical analogues of rainbow trapping and mode conversion. *New J. Phys.* **20**, 053017 (2018).
8. L. Chen, G. P. Wang, Q. Gan, F. J. Bartoli, Rainbow trapping and releasing by

chirped plasmonic waveguides at visible frequencies. *Appl. Phys. Lett.* **97**, 153115 (2010).

9. F. Ding, Y. Jin, B. Li, H. Cheng, L. Mo, S. He, Ultrabroadband strong light absorption based on thin multilayered metamaterials. *Laser Photonics Rev.* **8**, 946–953 (2014).
10. Y. Cui, K. H. Fung, J. Xu, H. Ma, Y. Jin, S. He, N. X. Fang, Ultrabroadband Light Absorption by a Sawtooth Anisotropic Metamaterial Slab. *Nano Lett.* **12**, 1443–1447 (2012).
11. H. Hu, D. Ji, X. Zeng, K. Liu, Q. Gan, Rainbow Trapping in Hyperbolic Metamaterial Waveguide. *Sci. Rep.* **3**, 1249 (2013).
12. V. Romero-García, R. Picó, A. Cebrecos, V. J. Sánchez-Morcillo, K. Staliunas, Enhancement of sound in chirped sonic crystals. *Appl. Phys. Lett.* **102**, 091906 (2013).
13. U. Langbein, F. Lederer, T. Peschel, U. Trutschel, D. Mihalache, Nonlinear transmission resonances at stratified dielectric media. *Phys. Rep.* **194**, 325–342 (1990).
14. U. Langbein, F. Lederer, H.-E. Ponath, Generalized dispersion relations for nonlinear slab-guided waves. *Opt. Commun.* **53**, 417–420 (1985).
15. H. Takahashi, S. Suzuki, K. Kato, I. Nishi, Arrayed-waveguide grating for

wavelength division multi/demultiplexer with nanometre resolution. *Electron. Lett.*

26, 87–88 (1990).

16. M. S. Jang, H. Atwater, Plasmonic Rainbow Trapping Structures for Light Localization and Spectrum Splitting. *Phys. Rev. Lett.* **107**, 207401 (2011).
17. A. Colombi, V. Ageeva, R. J. Smith, A. Clare, R. Patel, M. Clark, D. Colquitt, P. Roux, S. Guenneau, R. V. Craster, Enhanced sensing and conversion of ultrasonic Rayleigh waves by elastic metasurfaces. *Sci. Rep.* **7**, 6750 (2017).
18. Q. Gan, Y. Gao, K. Wagner, D. Vezhenov, Y. J. Ding, F. J. Bartoli, Experimental verification of the rainbow trapping effect in adiabatic plasmonic gratings. *Proc. Natl. Acad. Sci.* **108**, 5169–5173 (2011).
19. Q. Gan, Y. J. Ding, F. J. Bartoli, “Rainbow” Trapping and Releasing at Telecommunication Wavelengths. *Phys. Rev. Lett.* **102**, 056801 (2009).
20. N. Kazemi-Zanjani, M. Shayegannia, R. Prinja, A. O. Montazeri, A. Mohammadzadeh, K. Dixon, S. Zhu, P. R. Selvaganapathy, A. Zavodni, N. Matsuura, N. P. Kherani, Multiwavelength Surface-Enhanced Raman Spectroscopy Using Rainbow Trapping in Width-Graded Plasmonic Gratings. *Adv. Opt. Mater.* **6**, 1701136 (2018).
21. K. L. Tsakmakidis, O. Hess, R. W. Boyd, X. Zhang, Ultraslow waves on the nanoscale. *Science*. **358**, eaan5196 (2017).

22. R. J. P. Engelen, D. Mori, T. Baba, L. Kuipers, Two Regimes of Slow-Light Losses Revealed by Adiabatic Reduction of Group Velocity. *Phys. Rev. Lett.* **101**, 103901 (2008).
23. H. Kurt, D. Yilmaz, Rainbow trapping using chirped all-dielectric periodic structures. *Appl. Phys. B.* **110**, 411–417 (2013).
24. A. Arreola-Lucas, G. Báez, F. Cervera, A. Climente, R. A. Méndez-Sánchez, J. Sánchez-Dehesa, Experimental Evidence of Rainbow Trapping and Bloch Oscillations of Torsional Waves in Chirped Metallic Beams. *Sci. Rep.* **9**, 1860 (2019).
25. S. He, Y. He, Y. Jin, Revealing the truth about ‘trapped rainbow’ storage of light in metamaterials. *Sci. Rep.* **2**, 00583 (2012).
26. A. Reza, M. M. Dignam, S. Hughes, Can light be stopped in realistic metamaterials? *Nature.* **455**, E10–E11 (2008).
27. K. L. Tsakmakidis, A. D. Boardman, O. Hess, Tsakmakidis et al. reply. *Nature.* **455**, E11–E12 (2008).
28. X. Zhang, D. Ö. Guney, Adverse effect of material absorption on stopped light hollow waveguides with negative index metamaterial cladding. *JOSA B.* **36**, 248–255 (2019).
29. K. Liu, S. He, Truly trapped rainbow by utilizing nonreciprocal waveguides. *Sci.*

Rep. **6**, 30206 (2016).

30. V. S. Asadchy, I. A. Faniayeu, Y. Ra'di, S. A. Khakhomov, I. V. Semchenko, S. A. Tretyakov, Broadband Reflectionless Metasheets: Frequency-Selective Transmission and Perfect Absorption. *Phys. Rev. X* **5**, 031005 (2015).
31. M. A. Morgan, T. A. Boyd, Theoretical and Experimental Study of a New Class of Reflectionless Filter. *IEEE Trans. Microw. Theory Tech.* **59**, 1214–1221 (2011).
32. M. Khalaj-Amirhosseini, M. Taskhiri, Twofold Reflectionless Filters of Inverse-Chebyshev Response With Arbitrary Attenuation. *IEEE Trans. Microw. Theory Tech.* **65**, 4616–4620 (2017).
33. R. Gómez-García, J. Muñoz-Ferreras, W. Feng, D. Psychogiou, Balanced Symmetrical Quasi-Reflectionless Single-and Dual-Band Bandpass Planar Filters. *IEEE Microw. Wirel. Compon. Lett.* **28**, 798–800 (2018).
34. M. A. Morgan, T. A. Boyd, Reflectionless Filter Structures. *IEEE Trans. Microw. Theory Tech.* **63**, 1263–1271 (2015).
35. J. Shi, Z. Xu, X. Yin, Broadband-rejection filter topology with a reflectionless feature inspired by the orthogonal distribution of gradual-changing artificial transmission structures. *Appl. Phys. Express.* **12**, 074501 (2019).
36. Z. Xu, H. Zhao, X. Yin, New filter topology with a reflectionless feature based on slow-wave structures loaded with resonator arrays. *Jpn. J. Appl. Phys.* **58**, 030913

(2019).

37. A. Pors, M. G. Nielsen, R. L. Eriksen, S. I. Bozhevolnyi, Broadband Focusing Flat Mirrors Based on Plasmonic Gradient Metasurfaces. *Nano Lett.* **13**, 829–834 (2013).
38. Y. Xu, Y. Fu, H. Chen, Planar gradient metamaterials. *Nat. Rev. Mater.* **1**, 16067 (2016).
39. D. Lin, P. Fan, E. Hasman, M. L. Brongersma, Dielectric gradient metasurface optical elements. *Science*. **345**, 298–302 (2014).
40. Z. Li, M.-H. Kim, C. Wang, Z. Han, S. Shrestha, A. C. Overvig, M. Lu, A. Stein, A. M. Agarwal, M. Lončar, N. Yu, Controlling propagation and coupling of waveguide modes using phase-gradient metasurfaces. *Nat. Nanotechnol.* **12**, 675–683 (2017).
41. S. Lannebère, M. G. Silveirinha, Optical meta-atom for localization of light with quantized energy. *Nat. Commun.* **6**, 8766 (2015).
42. D. A. Powell, Interference between the Modes of an All-Dielectric Meta-atom. *Phys. Rev. Appl.* **7**, 034006 (2017).
43. A. K. Ospanova, G. Labate, L. Matekovits, A. A. Basharin, Multipolar passive cloaking by nonradiating anapole excitation. *Sci. Rep.* **8**, 12514 (2018).
44. L. Wei, Z. Xi, N. Bhattacharya, H. P. Urbach, Excitation of the radiationless anapole mode. *Optica*. **3**, 799 (2016).

45. J. D. Baena, J. Bonache, F. Martin, R. M. Sillero, F. Falcone, T. Lopetegui, M. A. G. Laso, J. Garcia-Garcia, I. Gil, M. F. Portillo, M. Sorolla, Equivalent-circuit models for split-ring resonators and complementary split-ring resonators coupled to planar transmission lines. *IEEE Trans. Microw. Theory Tech.* **53**, 1451–1461 (2005).
46. R. G. Quarfoth, D. F. Sievenpiper, Nonscattering Waveguides Based on Tensor Impedance Surfaces. *IEEE Trans. Antennas Propag.* **63**, 1746–1755 (2015).
47. J. Lee, D. F. Sievenpiper, Method for Extracting the Effective Tensor Surface Impedance Function From Nonuniform, Anisotropic, Conductive Patterns. *IEEE Trans. Antennas Propag.* **67**, 3171–3177 (2019).
48. Z. Xu, X. Yin, D. F. Sievenpiper, Adiabatic Mode-Matching Techniques for Coupling Between Conventional Microwave Transmission Lines and One-Dimensional Impedance-Interface Waveguides. *Phys. Rev. Appl.* **11**, 044071 (2019).
49. D. J. Bisharat, D. F. Sievenpiper, Guiding Waves Along an Infinitesimal Line between Impedance Surfaces. *Phys. Rev. Lett.* **119**, 106802 (2017).
50. A. Gopinath, Maximum Q-Factor of Microstrip Resonators. *IEEE Trans. Microw. Theory Tech.* **29**, 128–131 (1981).
51. R. Azadegan, K. Sarabandi, Miniature high-Q double-spiral slot-line resonator filters. *IEEE Trans. Microw. Theory Tech.* **52**, 1548–1557 (2004).
52. J. B. Khurgin, How to deal with the loss in plasmonics and metamaterials. *Nat.*

Nanotechnol. **10**, 2–6 (2015).

- 53. T. Lu, J. Jin, Electrical-Thermal Co-Simulation for Analysis of High-Power RF/Microwave Components. *IEEE Trans. Electromagn. Compat.* **59**, 93–102 (2017).
- 54. E. Shamonina, V. A. Kalinin, K. H. Ringhofer, L. Solymar, Magnetoinductive waves in one, two, and three dimensions. *J. Appl. Phys.* **92**, 6252–6261 (2002).
- 55. Z. Xu, S. Liu, S. Li, H. Zhao, L. Liu, X. Yin, Tunneling of spoof surface plasmon polaritons through magnetoinductive metamaterial channels. *Appl. Phys. Express.* **11**, 042002 (2018).
- 56. L. Solymar, E. Shamonina, *Waves in Metamaterials* (OUP Oxford, 2009).
- 57. E. Shamonina, Magnetoinductive polaritons: Hybrid modes of metamaterials with interelement coupling. *Phys. Rev. B.* **85**, 155146 (2012).